Progress In Electromagnetics Research B, Vol. 53, 241–266, 2013

DESIGN AND MEASUREMENT-BASED EVALUATION OF MULTI-ANTENNA MOBILE TERMINALS FOR LTE 3500 MHz BAND

Abdullah Al-Hadi Azremi[1, 3, *], Nima Jamaly[2], Katsuyuki Haneda[1], Clemens Icheln[1], and Ville Viikari[1]

[1]Department of Radio Science and Engineering, School of Electrical Engineering, Aalto University, Espoo, Finland

[2]Department of Signals and Systems, Chalmers University of Technology, Gothenburg, Sweden

[3]School of Computer and Communication Engineering, Universiti Malaysia Perlis, Perlis, Malaysia

Abstract—Design of multi-element antennas (MA) for small mobile terminals operating at higher frequencies remains challenging despite smaller antenna dimension and possibility of achieving electrically large separation between them. In this paper, the importance of the type of radiating elements operating at 3400–3600 MHz and their locations on the terminal chassis is highlighted. An isotropic radiation pattern that receives incoming signals from arbitrary directions is obtained by combining the radiation patterns of multiple antennas with localized chassis current distribution. Four MA configurations with two- and eight-element antennas are designed and evaluated experimentally in indoor propagation environments. Our proposed designs of MAs provide the highest MIMO channel capacity compared to their counterparts using antennas with less localized chassis current distribution, even in the presence of user's hand.

1. INTRODUCTION

Increasing the number of antennas in small mobile terminals is widely known as an option to enhance the performance of MIMO mobile terminals [1–5]. On the base station side, link capacity can be improved by employing multiple antennas without space restrictions [6]. In contrast, compact terminal antennas are strictly limited in size.

Received 12 June 2013, Accepted 31 July 2013, Scheduled 2 August 2013

* Corresponding author: Abdullah Al-Hadi Azremi (abdullah.azremi@aalto.fi).

Mutual coupling often exists among antenna elements, and increases significantly as the number of elements increases [5]. In addition to this, the way a user holds the mobile terminal affects the overall performance [7, 8].

Extensive research has been done in the recent years to study different methods to mitigate mutual coupling between two closely spaced antennas, thus improving their MIMO performance [9, 10]. Earlier research mainly focuses on the relatively low frequency bands, such as Long Term Evolution (LTE) 700 MHz and GSM 900 MHz bands [11–13]. The main challenges were due to 1) the non-available electrical separation of 0.25λ between two antennas and 2) mobile terminal chassis radiation due to the dominant characteristic mode of the terminal chassis [10, 14]. These two challenges are not crucial at frequencies above 3000 MHz, since the required antenna separation can be achieved easily and contribution of terminal chassis is not significant. However, determining the type of radiating elements and choosing the antenna locations on the terminal chassis are important design aspects to be considered. When the frequency increases, fabrication of an antenna becomes more challenging. Hence, it is essential to improve the current understanding on the design of MA on mobile terminal especially for the 3400–3600 MHz LTE band [15].

The degradation of MIMO performance in the presence of user's hand has been the main concern in research [7, 8, 16, 17]. The effect of the user's hand is a further aspect requiring adequate consideration in the early design phase. Since the antennas are relatively small at 3500 MHz, placing the antennas at locations that are less obstructed by the user's hand is of interest. Therefore, placement of the antennas to minimize the effect of user's hand is investigated here.

This paper investigates different state-of-the-art antennas for the 3500 MHz band in compact mobile terminals. The effect of presence of one and two hands on the terminal and its impact on antenna location are studied. Based on these investigations, we propose antenna designs comprising of two- and eight-element antennas that achieve the highest MIMO channel capacity compared to their counterpart multi-antenna structures. We finally provide insights concerning impact of incorporating antennas in mobile terminal on MIMO performance, especially when the user's hand is present.

2. OVERVIEW OF MULTI-ANTENNA DESIGNS FOR MOBILE HANDSET

The terminal chassis formed by the Printed Circuit Board (PCB) and the metallic shielding is known to have a crucial role in the performance

of a small antenna in mobile handsets [14]. Parameters such as bandwidth, Specific Absorption Rate (SAR) and radiation efficiency depend largely on the terminal chassis resonances at frequencies below 2000 MHz [18]. However, the dependency of these parameters with the terminal chassis with size of 100 mm × 40 mm was shown not to be significant beyond 3000 MHz, where radiation from the antenna element itself becomes dominant [19]. For an MA system in this frequency range, the type of antenna element is important since realization of 0.25λ separation between two closely spaced antennas can be easily achieved.

This section presents an overview of state-of-the-art internal antenna designs which could be employed for MA system in mobile handset. We choose several internal antenna designs and then study their current distributions on the terminal chassis. The current distribution is investigated to gain an insight on mutual coupling when two or more antennas are incorporated into the same terminal [13]. Apart from elaborating on antenna characteristics of commonly used internal antennas, we also highlight the importance of considering the antenna locations on the terminal in the early design phase.

2.1. State-of-the-art Internal Antennas

The main types of internal antennas are resonant-based folded monopole antenna and Planar Inverted-F Antenna (PIFA) [20, 21]. In order for the folded monopole to be integrated in the housing of the mobile handset, the height of the monopole has to be very small and thus become capacitive, evolving into the Inverted-F Antenna (IFA) [22]. A non-resonant type Capacitive Coupling Element (CCE) antenna is also an interesting candidate for a low-profile internal handset antenna [23]. It is due to the simplicity of the coupling element geometry and flexibility offered by an external matching circuitry to match at any frequency of interest. At 3500 MHz, a lot of efforts have been made to design single or multiple antennas by using PIFA, monopole, IFA and CCE [24–28]. Also in this work, PIFA, IFA and CCE antenna types are investigated.

Each antenna type is designed to be operating at 3500 MHz, by meeting the matching criterion of input reflection coefficient $|S_{jj}| \leq -6$ dB across the LTE 3400–3600 frequency band. In the design of PIFA, the height between the ground plane and the radiating patch is 5 mm and the separation between the shorting and feeding plates is 1 mm. The CCE is an off-ground plane corner-type structure having 2 mm ground clearance, occupying 80 mm^3 volume. The CCE antenna element is matched at 3500 MHz using lumped components. A 85 mm^2 slot cut on the ground plane is dedicated for the IFA. The wire-type

IFA is protruded from the ground plane with a length of 20 mm and a width of 1.5 mm. All antenna elements have met the required matching criterion.

It was shown earlier that the corner edges of the terminal chassis were found to be optimal for couplers to excite the first three characteristic modes [29]. Hence, all antenna elements are optimally located at one of the corner edges to gain fair insights into the excited current distribution on the terminal chassis at 3500 MHz.

Figure 1 shows the geometries and normalized current distributions on the terminal chassis for different antenna elements. The normalization is performed against the overall peak current density of all three MA structures. Among the studied structures, it is found that the current of the PIFA is less localized than those of the IFA and CCE. The PIFA has the highest Q-factor of 9.0 compared to the IFA and CCE with Q of 7.7 and 8.5, respectively. Although the PIFA has stronger reactive near-field around the antenna element compared to the IFA and CCE, the current is distributed all over the terminal chassis as shown in Fig. 1(a).

The localized current of the IFA and CCE shows that the radiation

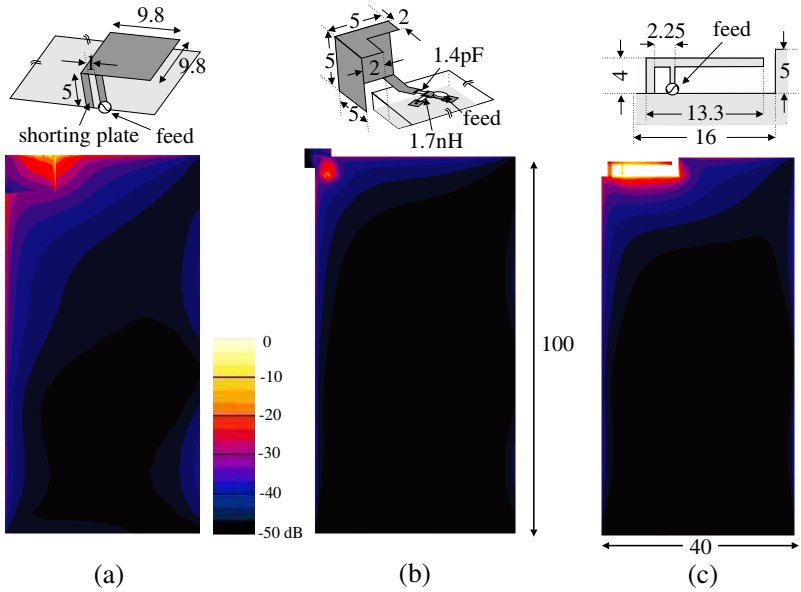

Figure 1. Antenna geometries and corresponding normalized magnitude of current distributions for (a) PIFA, (b) CCE and (c) IFA. All dimensions are in millimeters.

depends less on the terminal chassis, and thus leads to a lower mutual coupling if the main antenna is in the vicinity of other localized current antenna(s) [30]. On the other hand, PIFA was found to have localized currents at the 900 MHz band [13]. This indicates that current localization of specific antenna element behaves differently at different frequency ranges. The effectiveness of the current localization also largely depends on the geometry and size of the terminal chassis, and the type of the antenna.

2.2. Practical Design Considerations for Multiple Antennas in Mobile Handset

Placement of multiple antennas on a compact terminal chassis should take into account other related RF components too. Antenna placement on the terminal chassis is of great importance since different locations of antenna exhibit different radiation properties [21]. Therefore, locations around major and minor edges of the terminal chassis are practical for the placement of antenna elements, with the remaining locations left for other components such as RF devices and circuits, loudspeakers, camera, vibrators and battery. The available area for the placement of the antennas is shown in Fig. 2(a).

On the other hand, the mobile handsets are also used for data transfer or browsing scenarios wherein a user holds the terminal with either one or two hands [7, 28, 31]. In [32], the effects of hand grips on over-the-air performance were found to be very significant since a change in the position has led to an efficiency variation of about

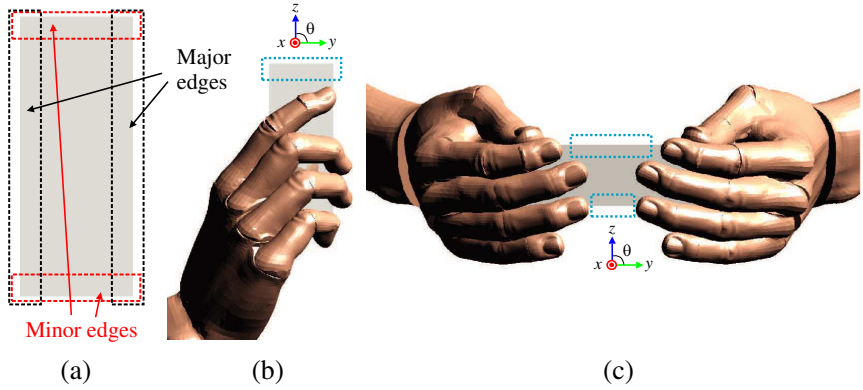

Figure 2. (a) Available antenna placement, and terminal chassis with user's (b) one hand, and (c) two hands. The blue dotted lines represent areas where antenna location is less obstructed with the user's hand.

4 dB. The antenna element that is in close proximity or covered by the user's hand suffers substantial detuning and power absorption by the hand [28, 32, 33]. Based on these two grips, the available space left for placing the antenna elements is limited as shown in Figs. 2(b) and 2(c), respectively.

In this work, the locations where the antenna elements are less obstructed with the user's hand are of interest. In order to employ two elements, having at least one element that is less obstructed in these hand grips is desirable. If the user holds the terminal using one hand, an antenna element is proposed to be at the top corner of the minor edge of the terminal chassis. Meanwhile, the second antenna element is proposed to be located at the center of the terminal's major edge to minimize the effect of user's holding terminal with two hands. Similar practical consideration for antenna placement of a terminal with large number of antennas, e.g., eight-element is also applied, which will be shown in the next section.

3. MULTI-ANTENNA DESIGNS UNDER STUDY

This section gives an overview of the antenna design specifications used in this work. We start by describing our proposed designs and continue with reference multi-antenna structures used for comparison. The antenna placement for all structures are chosen based on the practical design consideration summarized in the previous section. The design concept is validated through extensive simulations by a commercial software from SPEAG [34]. The whole antenna structure is modelled as a perfect electric conductor (PEC), and hence the source of losses in the antenna is only due to mismatch and mutual coupling between antenna elements.

3.1. Proposed Compact Multi-antenna Structures

Based on the investigation made in Section 2.1, we propose combination of two different types of antenna with localized chassis current distribution, i.e., the CCE and IFA as antenna elements in our two-element structure. The configuration of the proposed structure referred to as '2-CF' is shown in Fig. 3(a). We use the CCE antenna at one chassis corner, and the IFA in the center of one of the long chassis edges. The CCE is a non-resonant structure, i.e., the resonance of the antenna is not based on the geometry but it is created by a matching circuit. The matching circuit consisting of a lumped inductor and a capacitor is used in order to create the antenna resonance at 3500 MHz. From Fig. 1(c), the cut slot ground plane of the IFAs has reduced the

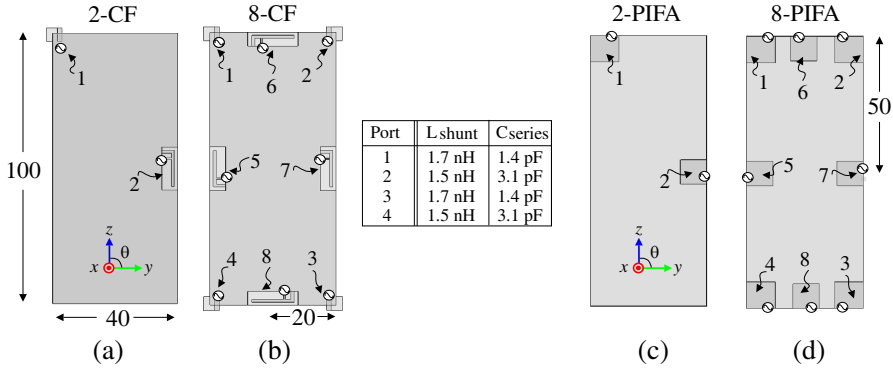

Port	L shunt	C series
1	1.7 nH	1.4 pF
2	1.5 nH	3.1 pF
3	1.7 nH	1.4 pF
4	1.5 nH	3.1 pF

Figure 3. Proposed MA configurations (a) '2-CF', (b) '8-CF', and PIFA-based MA configurations as reference structure (c) '2-PIFA', (d) '8-PIFA'. All dimensions are in millimeter.

coupling effect from the terminal chassis.

An eight-element antenna structure referred to as '8-CF' is shown in Fig. 3(b). It comprises of four CCEs at each chassis corner, and four differently oriented IFAs around the chassis. The values for matching components used to match four CCEs are shown in the table next to Fig. 3(b). The size of the CCEs and the IFAs are the same as in the '2-CF'.

3.2. Planar Inverted-F Antenna Structures

In comparison with the proposed antenna designs described in Section 3.1, simple and practical identical PIFAs are designed as reference MA structures. The configurations of the two- and eight-element PIFAs are shown in Figs. 3(c) and 3(d), respectively. The radiating plate dimensions are kept the same, i.e., 9.8 mm × 9.8 mm for all structures under study, except for the reduced size of element 7 and 8 in '8-PIFA' with 9.0 mm × 9.0 mm so that the PIFAs meet the same matching criterion.

4. ANTENNA-CHANNEL SYNTHESIS AND EVALUATION METRICS

In this section, we describe how simulated radiation patterns of MAs can be used in conjunction with the measured multipath data to calculate the performance metrics. We first explain the measurement - based antenna testbed, and thereafter provide some useful information

on normalization of the data. The second part is dedicated to describe performance metrics used for evaluating the antennas under study.

4.1. Measurement-based Antenna TestBed

Performance evaluation of the MAs presented in this work is based on the principle of combining simulated radiation patterns with multiple plane waves from measured propagation channels. The tool called Measurement-Based Antenna TestBed (MEBAT) was developed and discussed in detail in [35], and was used extensively for MAs performance evaluation in [36]. The radio channels used in this work were from an extensive double directional TKK Radio Channel Measurements database, previously obtained for 5300 MHz frequency band. The database was used for the evaluation of MAs designed at 3500 MHz with an assumption that the small-scale fading statistics, i.e., the distribution of propagation paths over the angular and delay domains, do not change significantly between the two radio frequencies. The same assumption is made, for example, in the WINNER II channel model [37] that defines the same small-scale fading statistics over the frequency range from 2000 to 6000 MHz. However, generality of the assumption for different propagation environments are still not properly justified. We chose the 5300 MHz data because they are the propagation channels measured at the closest radio frequency to our MAs design. Details of the propagation measurement's sounder can be found in [38].

The Base Station (BS) antenna used in this work is a computational two-element uncorrelated dual-polarized isotropic antenna. The antennas are located 0.5λ apart from each other. This ensures a fairly good representation to minimize the effect of non-uniform radiation pattern at the BS side.

The combination of simulated MAs 3D-radiation patterns at the BS and Mobile Station (MS) with measured plane waves results in a MIMO channel matrix, as a function of mobile locations travelling along various routes. Since the same set of radio channel propagation data were used for all the MA structures under study, the variations in the results are caused by differences in the MAs radiation patterns and orientations only.

The mobile terminals in actual multipath environments may have arbitrary orientations in space, e.g., in azimuth plane or the elevation angle [36, 39]. In this work, arbitrary rotation effects is simulated by rotating the radiation pattern in 60° steps in azimuth plane, at each elevation angles of 30° and 60°, respectively. The proposed rotation scheme results in a total of 12 antenna orientations for each MA at each location along the route. The MIMO channel matrices were

computed for each orientation at all MS locations along the route. Hence, the number of channel matrices was $12N_S$ (N_S refers to number of MS locations along the route) allowing the statistical analysis of the evaluation metrics [36]. In MEBAT, the power normalization of the channel matrices was performed by antenna-independent power normalization method [39].

An ideal isotropic antenna is shown to be useful reference in MIMO performance evaluation [35, 36, 40]. A computational two-element uncorrelated antenna referred to as '2-ISO' is used for power normalization. The '2-ISO' antenna is shown in Fig. 4(a). Both elements are dual-polarized isotropic antennas. The '2-ISO' is virtually moving along the same measurement routes. The resultant channel matrices obtained with the MAs were normalized with the total received power by the '2-ISO' structure. For comparison with the proposed eight-element structures, an eight-element uncorrelated dual-polarized antenna referred to as '8-ISO' is used, as illustrated in Fig. 4(b). The locations of the '2-ISO' and '8-ISO' antenna elements are the same as those of the two- and eight-element antennas shown in

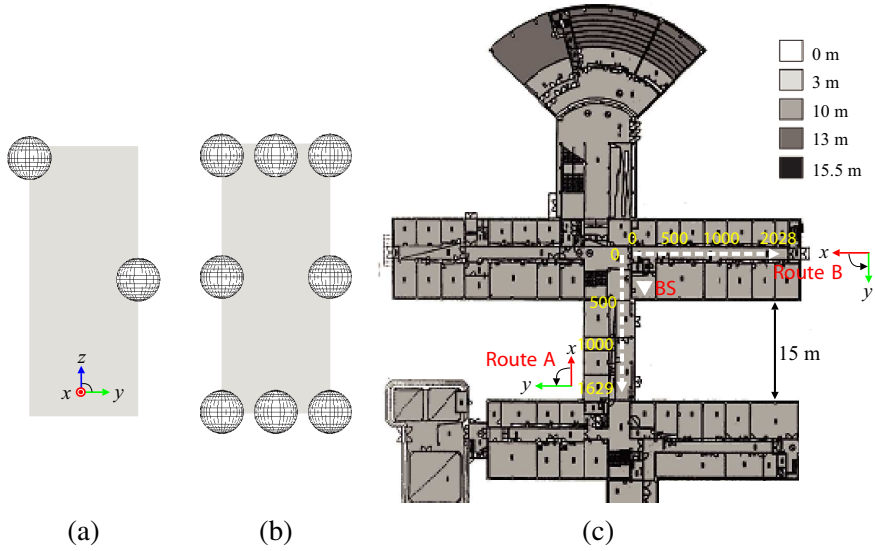

Figure 4. (a) '2-ISO' antenna used for power normalization, (b) '8-ISO' antenna, and (c) obstructed Line-of-Sight (Route A) and non Line-of-Sight (Route B) scenarios. The triangle represents BS location while the arrows are mobile routes. The X axes indicate the direction of MS in 0° azimuth angle.

Fig. 3.

Two scenarios in indoor measured propagation routes have been considered, as shown in Fig. 4(c). In both routes, the BS was located in one room. The measured MS locations along the routes for Route A and B were 1629 and 2028 locations, respectively. Both BS and MS heights were 1.6 m from the floor.

Angular power spectrums of the multipath for the two routes are shown in Figs. 5(a) and 5(b), respectively. Dominant propagation mechanism for the two measurement routes is typical directive wave guidance through the corridor. The directive power angular spectrum is more common in indoor scenarios compared to uniformly distributed power spectrum.

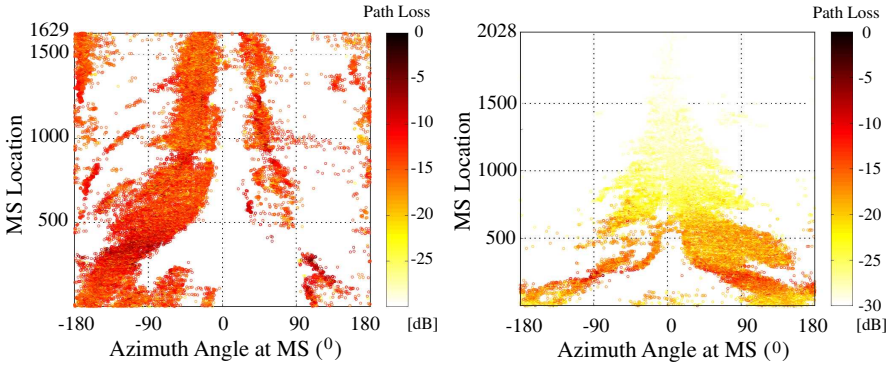

Figure 5. Angular power spectrum (normalized path loss) for (a) Route A and (b) Route B. The maximum number of multipath components per MS location is 30.

4.2. Performance Metrics

4.2.1. Mean Matching Efficiency, Electromagnetic Mutual Coupling and Cross Polarization Discrimination

In an N-multiple antenna system, the total embedded element efficiency of, say, k-th port is the ratio between the total radiated power and the maximum available power from the source when the foregoing port is excited while other ports are terminated [41]. This metric takes into account both 'multiport matching efficiency' and the embedded radiation efficiency associated with each port [42].

In short, total embedded element efficiency e_{tot} is the extension to a multiport case from the classical total efficiency for single-element antenna. To further simplify the evaluation, we use a single efficiency

metric called mean matching efficiency, e_{mm} [42]. This efficiency is obtained by taking the geometric mean of all total embedded element efficiencies, across the 3400–3600 MHz band:

$$e_{\mathrm{mm}} = \left(\prod_{k=1}^{N} e_{\mathrm{tot}}^{k} \right)^{\frac{1}{N}}. \tag{1}$$

The concept of electromagnetic mutual coupling, EM_{coup} is used to compare mutual coupling of different multi-antenna designs, which excludes the effect of impedance matching [43]. The EM_{coup} defines the mutual coupling when both ports of a two-port network are conjugate matched [44].

Cross-polarization discrimination, *XPD* is used to evaluate the polarization state of each antenna element, which relates to polarization diversity [45]. It is defined as the ratio between gains, at main and cross polarizations.

4.2.2. MIMO Channel Capacity and Transferred Signal Power

MIMO channel capacity for the i-th mobile location along the route, $C^{(i)}$ can be expressed as [35, 36, 40]:

$$C^{(i)} = \log_2 \left[\det \left(\mathbf{I} + \frac{\rho}{n_{\mathrm{T}}} \frac{\mathbf{H}_{\mathrm{AUT}}^{(i)} \left(\mathbf{H}_{\mathrm{AUT}}^{(i)} \right)^{\mathrm{H}}}{P_{\mathrm{norm}}} \right) \right], \tag{2}$$

where $\mathbf{I}$ is an identity matrix, ρ the mean Signal-to-Noise Ratio (SNR) at the Mobile Station (MS), n_{T} the number of transmitting antennas, and $()^{\mathrm{H}}$ the Hermitian transpose. MIMO channel matrix, $\mathbf{H}_{\mathrm{AUT}}$, includes the effect of the simulated antenna patterns at both base and mobile stations. As mentioned in the preceding subsection, the computational '2-ISO' structure give the reference power for normalization, P_{norm}, which is calculated at each mobile measurement point. The power normalization at the i-th mobile location can be expressed as [35]:

$$P_{\mathrm{norm}} = \frac{1}{n_{\mathrm{T}} n_{\mathrm{R}}} \left\| \mathbf{H}_{\mathrm{ref}}^{(i)} \right\|_F^2, \tag{3}$$

where $\|.\|_F$ is the Frobenius norm, n_{R} the number of receiving antennas, and $\mathbf{H}_{\mathrm{ref}}$ the channel matrix with the two isotropic antennas at the BS and the '2-ISO' at the MS, respectively. Slow fading effect has been removed with sliding average of the instantaneous total power received over the mobile routes by the '2-ISO' in the same environment.

The length of the sliding window is 101, which corresponds to 1.2 m in mobile travelling distance along the route [35].

The MIMO channel capacity is also affected by the distribution of the eigenvalues of $\mathbf{H}_{\mathrm{AUT}}^{(i)}(\mathbf{H}_{\mathrm{AUT}}^{(i)})^{\mathrm{H}}$ [2]. Theoretically, an increase of relative spread between the eigenvalues means an increase in spatial correlation between antenna elements, thus far from being optimum with equal eigenvalues [46].

The ability to transfer signal power between the two ends of the link is determined by losses in a channel, antenna radiation properties and orientations. The instantaneous transferred signal power (TSP) of the MA system is defined as [40]:

$$TSP_{\mathrm{AUT}}^{(i)} = \frac{\left\|\mathbf{H}_{\mathrm{AUT}}^{(i)}\right\|_F^2}{\left\|\mathbf{H}_{\mathrm{ref}}^{(i)}\right\|_F^2}. \tag{4}$$

5. RESULTS AND DISCUSSIONS

In this section, we first investigate the scattering parameters, efficiency, cross polarization discrimination and radiation pattern characteristics of the MAs under study. We then analyze the performance of the MAs in nonuniform multipath environments by means of TSP, eigenvalue distribution and MIMO channel capacity. Finally, the performance of the MAs in the presence of the user's hand is investigated.

5.1. Scattering Parameter, Efficiency and Cross-polarization Discrimination

Table 1 summarizes the scattering parameters of all studied MAs at 3400–3600 MHz. The maximum and minimum values of the impedance-matching and electromagnetic mutual coupling among all elements in the respective structure are listed. In general, all MAs satisfy the impedance-matching criterion, $|S_{jj}| \leq -6$ dB, but in the worst-case mutual coupling of $|EM_{\mathrm{coup},jk}| = -5.4$ dB is observed.

The worst mutual coupling of the two-element structures are relatively small, i.e., better than -15.4 dB due to the large spatial separation of the elements. In contrast, the worst mutual coupling in all eight-element structures is high. In this work, the impact of current localization on the mutual coupling at 3500 MHz is not significant 1) for two-element structures since the antenna separation is large, i.e., more than 0.25λ, and 2) for eight-element structures due to the additive impact of the mutual coupling from all eight antennas.

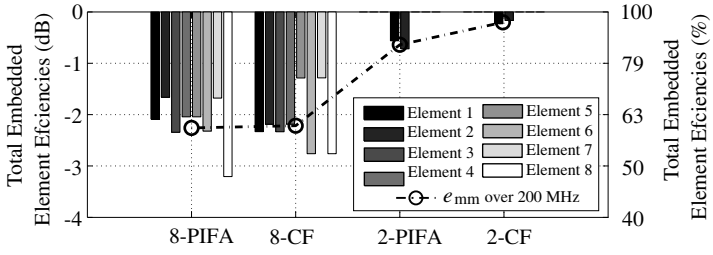

Figure 6. Total embedded element efficiencies at 3500 MHz, and mean matching efficiencies over 200 MHz bandwidth.

Figure 6 shows the total embedded element and mean matching efficiencies of the studied structures. It is shown that the '2-CF' achieved higher mean matching efficiencies compared to its counterpart, the '2-PIFA' structure by 0.6 dB. Since the electromagnetic mutual coupling over the bandwidth is relatively similar, the difference in total embedded element efficiency is mainly attributed to the improved matching efficiency by both antenna elements in the '2-CF' structure, shown in Table 1. The difference in the mean matching efficiencies for both eight-element structures is very small, only 0.02 dB. The additive impact of the mutual coupling in the eight-element structure have decreased the mean matching efficiency by about 1.6 dB compared to that of two-element structures.

Table 1. Minimum/Maximum Scattering Parameters of Studied MAs at 3400–3600 MHz.

MAs	Min/Max, $\lvert S_{jj}\rvert$ (dB)	Min/Max, $\lvert EM_{\mathrm{coup},jk}\rvert$ (dB)
2-PIFA	−14.0/−7.0	−18.4/−15.4
2-CF	−30.2/−12.4	−18.6/−16.1
8-PIFA	−26.0/−6.1	−35.9/−5.4
8-CF	−32.1/−10.6	−29.5/−5.7

Table 2. Cross polarization discrimination at 3500 MHz.

	Antenna XPDs (dB)								
MAs	1	2	3	4	5	6	7	8	$XPD_{\max} - XPD_{\min}$
2-PIFA	3.5	−1.0							4.5
2-CF	−2.3	3.5							5.8
8-PIFA	−1.8	5.3	−2.1	5.3	−3.6	−2.4	−2.4	−6.4	11.7
8-CF	−1.0	3.9	−1.0	3.9	2.3	−0.7	2.3	−0.7	4.9

Table 2 summarizes the cross polarization discrimination, *XPD* of all elements of the studied MAs at 3500 MHz. The '2-CF' structure obtained the highest variation in *XPD* between the elements of the two-element structures. However, the combination of CCE and IFA in the '8-CF' does not facilitate them to obtain the highest variation in *XPD* of the eight-element structures. In general, the mutual coupling from all eight antennas affects the polarization of all antennas in the eight-element structure.

5.2. Radiation Patterns

It is well known that the shapes of the MA's radiation pattern for different orientations and polarizations is important in estimating MIMO performance, especially when the incoming signal is non-uniformly distributed [36]. An MA system with an isotropic radiation pattern receives incoming signals from all directions. The degree of similarity between the studied MAs and the ideal isotropic radiation pattern can be assessed by means of combining the radiation patterns of each antenna element, when all antennas are excited. For fair comparison, the gains are normalized to a total input power of 1 W distributed to all antennas.

In order to observe the impact of localized current distribution on the radiation pattern, the gain of each antenna element in the presence and absence of the second antenna element is investigated. Both cases are shown in Fig. 7, denoted by 'AntennaNumber' and 'AntennaNumber only', respectively. It shows that both the CCE and IFA in the '2-CF' structure maintain their radiation patterns when

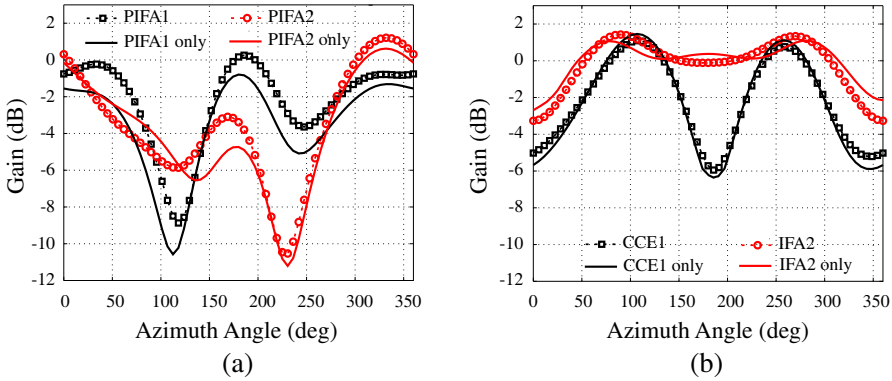

Figure 7. Azimuthal (*xy*-plane) gain pattern for (a) '2-PIFA' and (b) '2-CF'.

the second antenna element is added on the same terminal chassis. However, the embedded element pattern of the '2-PIFA' structure changes more when the second element is added. It indicates higher tolerance of the current localized antennas to the presence of other antennas on the same terminal chassis.

In the '2-CF' structure, the beam-width of the combined radiation pattern is increased and thus yields a more isotropic pattern compared to the '2-PIFA' structure. The main mechanism is due to the localized current distributions of the IFA and CCE on the terminal chassis. When the current is localized, it seems to be easier to exploit pattern, spatial and angle diversities independently. Additionally, different antenna geometry provide dissimilarities of the radiation patterns.

The normalized combined radiation pattern for two- and eight-element structures are shown in Figs. 8 and 9, respectively. The gains

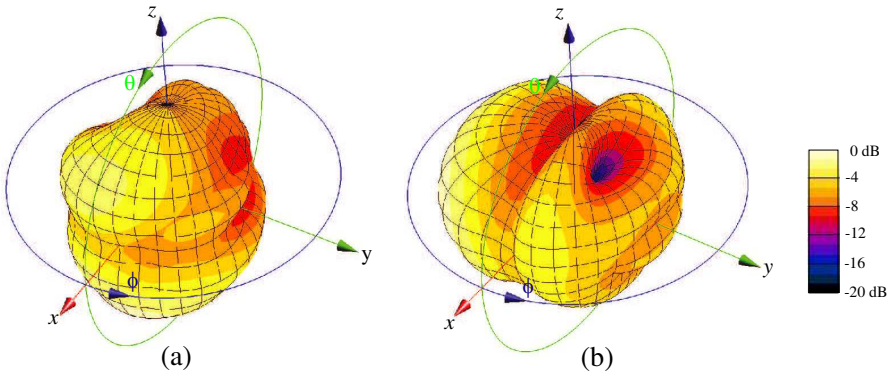

Figure 8. Combined normalized gain for (a) '2-PIFA' and (b) '2-CF'.

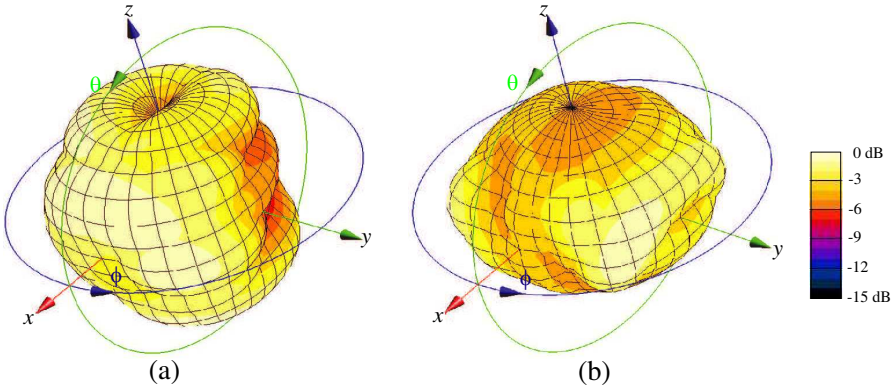

Figure 9. Combined normalized gain for (a) '8-PIFA' and (b) '8-CF'.

are normalized to the highest gain among the antenna elements. For the same reason, the combined radiation pattern of the '8-CF' is more isotropic compared to that of the '8-PIFA' structure. The combined radiation patterns from all PIFAs result in a directive pattern towards $\phi = 0°$. Other possible combinations such as PIFA-IFA and PIFA-CCE have been also investigated for the same purpose. Both have shown an increased uniformity in the radiation pattern compared to the '8-PIFA' structure. For brevity reason, only two extreme cases of antennas with 1) all localized and 2) all non-localized chassis current distributions; '8-CF' and '8-PIFA' structures are shown in this work.

5.3. MIMO Performance in Nonuniform Environments

Link performance metrics such as the *TSP* and MIMO channel capacity for arbitrary mobile terminal orientations are evaluated. Two cumulative distribution functions (CDF) levels with the SNR $\rho = 10\,\text{dB}$ for MIMO channel capacity have been used for the evaluation, taken at 1% and 50% probability levels.

Figure 10 shows that the *TSP* level of the MA system plays an essential role in achieving high MIMO channel capacity, as shown by the trend between the *TSP* and the MIMO channel capacity. The proposed antennas, i.e., '2-CF' and '8-CF', achieve higher MIMO channel capacity compared to the identical element of PIFA-based MAs counterparts at both probability levels.

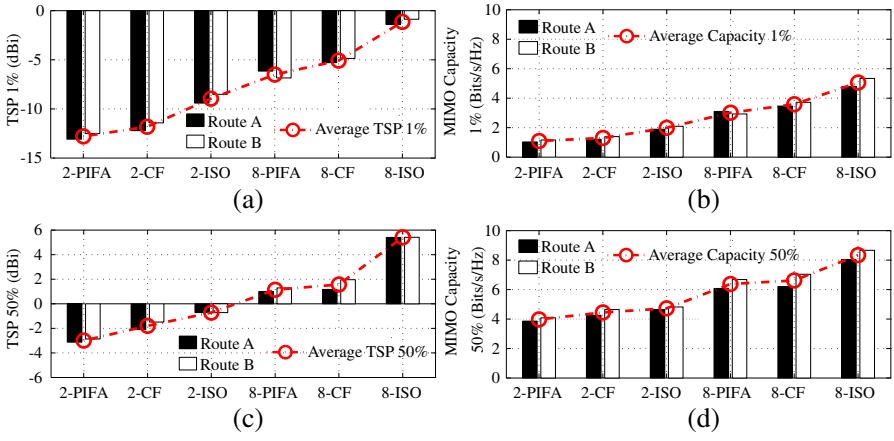

Figure 10. MAs performance ranking; at 1% probability level for (a) TSP, (b) MIMO channel capacity ($\rho = 10\,\text{dB}$) and at 50% probability level for (c) *TSP* and (d) MIMO channel capacity ($\rho = 10\,\text{dB}$).

At 1% probability level, the '2-CF' structure achieves 17% higher MIMO channel capacity than the '2-PIFA', and 45% less than that of the '2-ISO' reference structure. On the contrary, the '8-CF' structure achieves the highest MIMO channel capacity among studied MAs, 20% and 80% higher than that of the '8-PIFA' and '2-ISO', respectively. At the 50% probability level, the same trend is served with a smaller increment of MIMO channel capacities by '2-CF' and '8-CF'. The achieved improvements are 13% and 5% compared to '2-PIFA' and '8-PIFA', respectively.

An interesting observation from the evaluated *TSP* for different MAs is that the *TSP*s of '8-PIFA' and '8-CF' structures are positive values at the 50% probability level. The more isotropic radiation patterns of both '8-PIFA' and '8-CF' structures outperforming the uniform pattern (0 dBi gain) of the '2-ISO' by 1.8 dB and 2.3 dB, respectively.

For the specified propagation environments, the '8-ISO' outperforms all MAs and achieve the highest MIMO channel capacity at both probability levels. The improved design strategy of the '8-CF' by using antennas with localized chassis current distributions, different geometries and orientations leads to the best option in terms of MIMO channel capacity among studied practical MAs design. Although the mean matching efficiency was relatively similar, the '8-CF' structure is not designed for optimum embedded element efficiencies, rather for exhibiting different radiation pattern to exploit pattern and angle diversity from each antenna element. Evidently, MIMO channel capacity also depends on SNR level, the *TSP* and the spread between the eigenvalues of the MIMO channel matrix [36, 40].

The distributions of the eigenvalues obtained using the studied two- and eight-element MA configurations are shown in Figs. 11(a) and 11(b), respectively. It is worthwhile to mention that the number of eigenvalues for all studied MAs is the same, e.g., the minimum of $(n_{\mathrm{R}}, n_{\mathrm{T}})$. At 50% probability level, the spread between the two eigenvalues, i.e., difference between the first and second eigenvalues for the two-element MA structures; '2-ISO', '2-PIFA', '2-CF' are similar. For eight-element structures, the spreads are also similar although the '8-ISO' obtained higher power of eigenvalue distributions by about 3 dB, compared to the '8-PIFA' and '8-CF' structures. In general, adding more elements at the terminal increases the power of the two eigenvalues thus increases the MIMO channel capacity.

The similar spread of eigenvalues in the studied MAs suggests that the correlation level between antenna elements is also similar [36]. The results show that different designs of MA structures with the same number of antenna elements do not seem to affect the eigenvalue

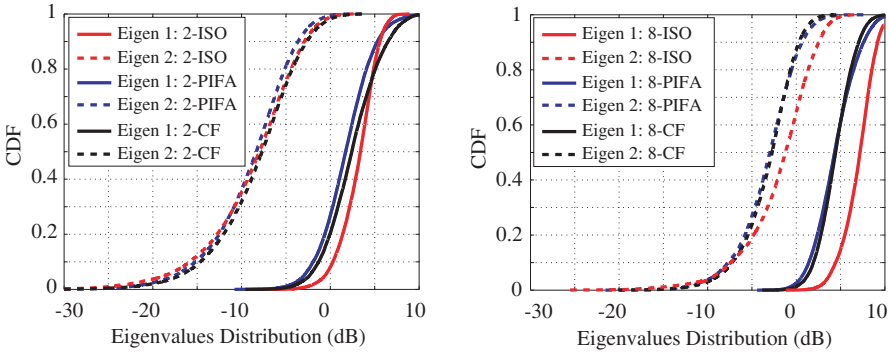

Figure 11. Eigenvalue distributions of the studied (a) 2×2 and (b) 2×8 MIMO systems in Route A.

distribution of a MIMO system. Therefore, the proposed '2-CF' and '8-CF' structures have mainly improved the *TSP* of the MIMO system and thus improved the MIMO channel capacity.

5.4. MIMO Performance in the Presence of Hand

Table 3 lists the scattering parameters of all studied MAs at 3400–3600 MHz in the presence of hand. In all structures, users hand detunes the resonance, and the worst-case mismatch is $|S_{jj}| = -4$ dB. In most investigated structures, the users hand lowers the mutual coupling, as shown earlier in Table 1. Fig. 12 shows the total embedded element and mean matching efficiencies of the studied MAs in the presence of hand. In addition to acceptable impedance-matching and mutual coupling in the presence of hand (refer to Table 3), these results suggest that the absorption loss is the main contributing factor in decreasing the mean matching efficiency.

Table 3. Minimum/maximum scattering parameters of studied MAs at 3400–3600 MHz in the presence of hand.

MAs	One-Hand		Two-Hands	
	Min/Max, $\lvert S_{jj}\rvert$ (dB)	Min/Max, $\lvert EM_{\text{coup},jk}\rvert$ (dB)	Min/Max, $\lvert S_{jj}\rvert$ (dB)	Min/Max, $\lvert EM_{\text{coup},jk}\rvert$ (dB)
2-PIFA	−10.7/−7.5	−20.5/−19.6	−4.4/−4.0	−30.2/−29.0
2-CF	−18.7/−9.8	−18.1/−17.8	−13.7/−5.7	−24.5/−20.6
8-PIFA	−42.8/−4.5	−50.1/−9.7	−9.5/−4.6	−50.6/−13.3
8-CF	−45.0/−9.0	−36.4/−9.6	−49.0/−6.5	−34.1/−8.4

Changes in the polarization state when the antenna is placed in the proximity of a human body have been found to affect the efficiency performance of a single-element antenna [47]. In this work, the *XPD*s of each antenna element in the presence of hand is investigated, and the values are listed in Table 4. It is found that there is no relation between the polarization and efficiency (see Fig. 12) of MAs in the presence of hand. A similar observation is made in the single-element antenna scenario [48].

The MIMO channel capacity of the studied MAs in the presence of hand is shown in Fig. 13. The user's hand grip used in the investigation is illustrated in Fig. 2. The MIMO channel capacity loss due to the user's hands exhibited a similar degradation for two-element structures,

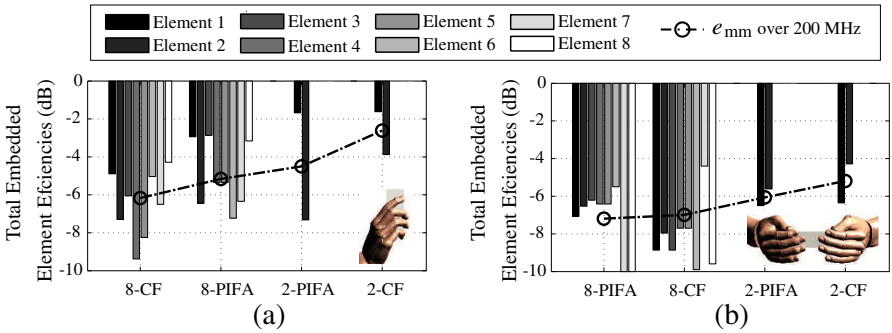

Figure 12. Total embedded element efficiencies at 3500 MHz, and mean matching efficiencies over 200 MHz bandwidth; with (a) one-hand and (b) two-hands.

Table 4. Cross polarization discrimination at 3500 MHz in the presence of hand.

	Antenna *XPD*s (dB) with One-Hand								
MAs	1	2	3	4	5	6	7	8	$XPD_{\max} - XPD_{\min}$
2-PIFA	−12.7	−12.9							0.2
2-CF	−12.2	4.4							16.6
8-PIFA	−7.9	−8.2	−5.3	−4.1	−15.3	−12.3	−30.0	9.9	39.9
8-CF	−7.4	4.2	1.2	−9.5	0.6	−0.4	1.7	−5.6	13.7
	Antenna *XPD*s (dB) with Two-Hands								
2-PIFA	7.4	15.9							8.5
2-CF	3.0	3.4							0.4
8-PIFA	9.2	8.8	7.9	6.2	−4.1	8.4	26.0	10.9	31.0
8-CF	−0.1	2.4	20.1	−2.0	−10.6	1.5	4.6	4.3	30.7

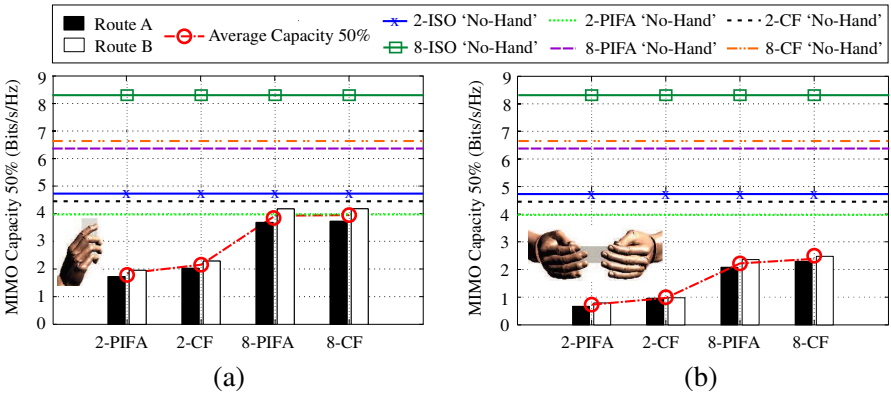

Figure 13. MAs performance ranking at 50% probability level for MIMO channel capacity ($\rho = 10$ dB); with (a) one-hand and (b) two-hands.

i.e., on an average, there is 53% and 80% reduction in the presence of one and two hands, respectively. Meanwhile, eight-element structures are degraded with 38% and 65% reduction for one and two hands, respectively. Among the studied MAs, it is shown that the degradation level is similar regardless of the type of antenna elements. Therefore, it is of considerable importance to achieve a high MIMO channel capacity already in the absence of hand.

On the other hand, the degradation is smaller when the structure is comprised of more antenna elements, i.e., the eight-element structure in the presence of the hand have more unobstructed antennas compared to the two-element structure. This is shown by having three out of eight antennas (elements 1, 2 and 7) unobstructed compared to only a single antenna (element 1) in the two-element structures in the presence of one hand. In the presence of two hands, two antennas (elements 5 and 6) and a single antenna (element 2) were unobstructed for eight- and two-element structures, respectively. Nevertheless, both proposed '2-CF' and '8-CF' structures reveal higher MIMO channel capacity than the '2-PIFA' and '8-PIFA', respectively.

Figure 14 shows the distributions of the eigenvalues obtained using the studied MAs in the presence of hand. Fig. 14(a) shows that there is a significant degradation in the power of eigenvalues by about 5 dB (one-hand) and 8 dB (two-hands), compared to the absence of hand (see Fig. 11). In the presence of one hand, first and second eigenvalues for two-element structures are decreased by 4 and 6 dB, respectively. Meanwhile in the presence of two hands, first and second eigenvalues are decreased by 7 and 9 dB, respectively. This suggest

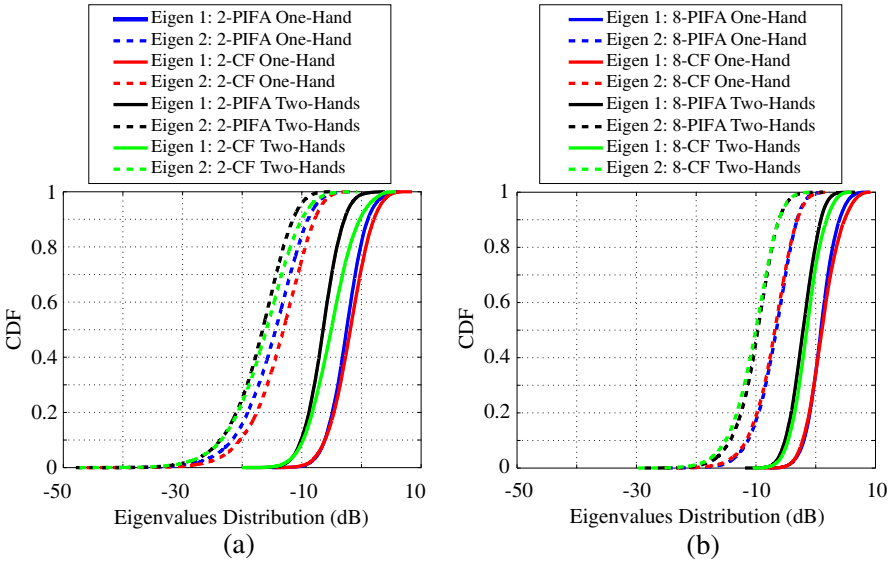

Figure 14. Eigenvalue distributions of the studied (a) 2×2 and (b) 2×8 MIMO systems in the presence of hand (Route A).

that the correlation level is lower compared to the absence of hand, as found earlier at 850 MHz and 2100 MHz in [49]. For eight-element structures (see Fig. 14(b)), it is found that the degradation of the first and second eigenvalues is similar, whereby reduction of 3.5 and 6.5 dB are obtained in the presence of one and two hands, respectively. In general, the 2×8 MIMO systems achieve higher power of eigenvalues for all user's hand scenarios, compared to the 2×2 MIMO systems. Additional antennas as in the eight-element structures facilitate more unobstructed antennas in the presence of hand. Nevertheless, the reduction in the power of eigenvalues due to the user's hand is similar for the studied MAs with the same amount of antennas.

It is well-accepted that increasing the number of antennas leads to an increase in complexity of the RF circuitry. Therefore, the improvement of MIMO channel capacity offered by incorporating more antenna elements comes at the expense of additional RF chains, that are difficult to implement on the relatively small mobile terminal chassis. In this work, it is observed that the degradation of MIMO channel capacity due to the presence of user's hand is reduced by only about 15%, when eight antennas is employed instead of two antennas. Moreover, it is achieved by adding complexity to the structure, with an addition of another 6 RF chains.

6. CONCLUSION

We have shown in this paper that the selection of a suitable radiating element plays a significant role to achieve good MIMO performance in compact mobile terminal operating at 3500 MHz. We experimentally show that the proposed designs that use CCE and IFA in the configuration exhibit good MIMO performance compared to the designs using only PIFAs as the radiating elements. Combining several antennas that have a localized chassis current distribution is shown to be one of the promising approaches to realize an almost isotropic radiation pattern. This work also highlights that antenna type, geometry, current distribution on the terminal chassis and radiation pattern of individual antenna element must be jointly considered in order to optimize the performance of a multi-antenna structure for mobile terminals.

For the studied MA configurations in the presence of a hand, it is found that the MIMO channel capacity degradation is similar regardless of the type of antenna element in the mobile terminal. It is shown that changes in polarization due to the effects of hand do not have a significant effect on MAs' total embedded element efficiencies. Antennas that are typically small in size at 3500 MHz can be flexibly placed at locations that are less obstructed by hands, since absorption losses are appreciable.

We have also shown that degradation of MIMO channel capacity due to the presence of user's hand is reduced by only about 15% by having additional 6 RF chains and antenna volume. Hence, increase the number of antennas above two may not be feasible by taking into account the added complexity. Compensation against the user's hand using antenna shielding [50] or by MIMO antenna selection [7, 28] are interesting topics left for future work.

ACKNOWLEDGMENT

The authors would like to thank Dr. V.-M. Kolmonen for providing the measured propagation channel data.

REFERENCES

1. Vaughan, R. and J. Andersen, "Antenna diversity in mobile communications," *IEEE Trans. Veh. Technol.*, Vol. 36, No. 4, 149–172, Nov. 1987.
2. Foschini, G. J. and M. J. Gans, "On limits of wireless communications in a fading environment when using multiple

antennas," *Wireless Pers. Commun.*, Vol. 6, No. 3, 311–335, Mar. 1998.

3. Jensen, M. and J. Wallace, "A review of antennas and propagation for MIMO wireless communications," *IEEE Trans. Antennas Propag.*, Vol. 52, No. 11, 2810–2824, Nov. 2004.
4. Geyi, W., "Multi-antenna information theory," *Progress In Electromagnetics Research*, Vol. 75, 11–50, 2007.
5. Karaboikis, M., V. Papamichael, G. Tsachtsiris, C. Soras, and V. Makios, "Integrating compact printed antennas onto small diversity/MIMO terminals," *IEEE Trans. Antennas Propag.*, Vol. 56, No. 7, 2067–2078, Jul. 2008.
6. Sulonen, K., P. Suvikunnas, L. Vuokko, J. Kivinen, and P. Vainikainen, "Comparison of MIMO antenna configurations in picocell and microcell environments," *IEEE J. Sel. Areas Commun.*, Vol. 21, No. 5, 703–712, Jun. 2003.
7. Harrysson, F., J. Medbo, A. Molisch, A. Johansson, and F. Tufvesson, "Efficient experimental evaluation of a MIMO handset with user influence," *IEEE Trans. Wireless Commun.*, Vol. 9, No. 2, 853–863, Feb. 2010.
8. Nielsen, J., B. Yanakiev, I. Bonev, M. Christensen, and G. Pedersen, "User influence on MIMO channel capacity for handsets in data mode operation," *IEEE Trans. Antennas Propag.*, Vol. 60, No. 2, 633–643, Feb. 2012.
9. Luxey, C. and D. Manteuffel, "Highly-efficient multiple antennasystems for small MIMO devices," *IEEE Int. Workshop Antenna Technol.*, 1–6, Mar. 2010.
10. Lau, B. K. and Z. Ying, "Antenna design challenges and solutions for compact MIMO terminals," *IEEE Int. Workshop Antenna Technol.*, 70–73, 2011.
11. Park, G., M. Kim, T. Yang, J. Byun, and A. Kim, "The compact quad-band mobile handset antenna for the LTE700 MIMO application," *IEEE Int. Symp. Antennas Propag. Society*, 1–4, 2009.
12. Bhatti, R.-A., S. Yi, and S.-O. Park, "Compact antenna array with port decoupling for LTE-standardized mobile phones," *IEEE Antennas Wireless Propag. Lett.*, Vol. 8, 1430–1433, 2009.
13. Li, H., Y. Tan, B. K. Lau, Z. Ying, and S. He, "Characteristic mode based tradeoff analysis of antenna-chassis interactions for multiple antenna terminals," *IEEE Trans. Antennas Propag.*, Vol. 60, No. 2, 490–502, Feb. 2012.
14. Vainikainen, P., J. Ollikainen, O. Kivekäs, and K. Kelander,

"Resonator-based analysis of the combination of mobile handset antenna and chassis," *IEEE Trans. Antennas Propag.*, Vol. 50, No. 10, 1433–1444, Oct. 2002.

15. 3GPP TR 37.801, "Technical specification group radio access network: UMTS-LTE 3500 MHz work item technical report," v10.0, Jan. 2011.
16. Plicanic, V., B. K. Lau, A. Derneryd, and Z. Ying, "Actual diversity performance of a multiband diversity antenna with hand and head effects," *IEEE Trans. Antennas Propag.*, Vol. 57, No. 5, 1547–1556, May 2009.
17. Azremi, A., J. Ilvonen, R. Valkonen, J. Holopainen, O. Kivekäs, C. Icheln, and P. Vainikainen, "Coupling element-based dualantenna structures for mobile terminal with hand effects," *Int. J. Wireless Inform. Networks*, Vol. 18, 146–157, 2011.
18. Kivekäs, O., J. Ollikainen, T. Lehtiniemi, and P. Vainikainen, "Bandwidth, SAR, and efficiency of internal mobile phone antennas," *IEEE Trans. Electromagn. Compat.*, Vol. 46, No. 1, 71–86, Feb. 2004.
19. Villanen, J., J. Poutanen, C. Icheln, and P. Vainikainen, "A wideband study of the bandwidth, SAR and radiation efficiency of mobile terminal antenna structures," *IEEE Int. Workshop Antenna Technol.*, 49–52, Mar. 2007.
20. Chen, Z. N., *Antennas for Portable Devices*, John Wiley & Sons, Ltd, 2007.
21. Fujimoto, K., *Mobile Antenna System Handbook*, Artech House, 2008.
22. Wong, K. L., *Planar Antennas for Wireless Communications*, Wiley Interscience, 2003.
23. Villanen, J., J. Ollikainen, O. Kivekäs, and P. Vainikainen, "Coupling element based mobile terminal antenna structures," *IEEE Trans. Antennas Propag.*, Vol. 54, No. 7, 2142–2153, Jul. 2006.
24. Pan, C.-Y., T.-S. Horng, W.-S. Chen, and C.-H. Huang, "Dual wideband printed monopole antenna for WLAN/WiMAX applications," *IEEE Antennas Wireless Propag. Lett.*, Vol. 6, 149–151, 2007.
25. Bhatti, R.-A., Y.-T. Im, and S.-O. Park, "Compact PIFA for mobile terminals supporting multiple cellular and non-cellular standards," *IEEE Trans. Antennas Propag.*, Vol. 57, No. 9, 2534–2540, 2009.
26. Ma, J., Y.-Z. Yin, J.-L. Guo, and Y.-H. Huang, "Miniature printed octaband monopole antenna for mobile phones," *IEEE Antennas*

Wireless Propag. Lett., Vol. 9, 1033–1036, 2010.

27. Lin, C.-R., T.-C. Hung, H.-H. Chiang, J.-H. Huang, J.-S. Chen, and Y.-C. Lin, "A novel open slot monopole antenna with a coupling element for WiMAX 3.5 GHz applications," *International Conference on Applications of Electromagnetism and Student Innovation Competition Awards*, 250–253, 2010.
28. Azremi, A., V. Papamichael, and P. Vainikainen, "Multi-antenna mobile terminal diversity performance in proximity to human hands under different propagation environment conditions," *Elect. Lett.*, Vol. 47, No. 22, 1214–1215, Oct. 27, 2011.
29. Martens, R., E. Safin, and D. Manteuffel, "Inductive and capacitive excitation of the characteristic modes of small terminals," *Loughborough Antennas Propag. Conf.*, 1–4, Nov. 2011.
30. Li, H., B. K. Lau, Y. Tan, S. He, and Z. Ying, "Impact of current localization on the performance of compact MIMO antennas," *Proc. 5th European Conf. Antennas Propag.*, 2423–2426, 2011.
31. Plicanic, V., H. Asplund, and B. K. Lau, "Performance of handheld MIMO terminals in noise- and interference-limited urban macrocellular scenarios," *IEEE Trans. Antennas Propag.*, Vol. 60, No. 8, 3901–3912, Aug. 2012.
32. Li, C.-H., E. Ofli, N. Chavannes, and N. Kuster, "Effects of hand phantom on mobile phone antenna performance," *IEEE Trans. Antennas Propag.*, Vol. 57, No. 9, 2763–2770, Sep. 2009.
33. Pelosi, M., O. Franek, M. Knudsen, M. Christensen, and G. Pedersen, "A grip study for talk and data modes in mobile phones," *IEEE Trans. Antennas Propag.*, Vol. 57, No. 4, 856–865, Apr. 2009.
34. "SEMCAD-X, a FDTD-based electromagnetic simulator," version 14.8 Aletsch, Schmid & Partner Engineering AG, Zurich, Switzerland, cited Oct. 1, 2012, Available: http://www.semcad.com.
35. Suvikunnas, P., J. Villanen, K. Sulonen, C. Icheln, J. Ollikainen, and P. Vainikainen, "Evaluation of the performance of multi-antenna terminals using a new approach," *IEEE Trans. Instrum. Meas.*, Vol. 55, No. 5, 1804–1813, Oct. 2006.
36. Villanen, J., P. Suvikunnas, C. Icheln, J. Ollikainen, and P. Vainikainen, "Performance analysis and design aspects of mobile-terminal multiantenna configurations," *IEEE Trans. Veh. Technol.*, Vol. 57, No. 3, 1664–1674, May 2008.
37. Kyösti, P., et al., "WINNER II channel models," Deliverable IST-WINNER D1.1.2 ver 1.1, European Commission, Sep. 2007, Available: http://projects.celticinitiative.org/winner+/WINNER2-Deliverables/.

38. Kolmonen, V.-M., J. Kivinen, L. Vuokko, and P. Vainikainen, "5.3-GHz MIMO radio channel sounder," *IEEE Trans. Instrum. Meas.*, Vol. 55, No. 4, 1263–1269, Aug. 2006.
39. Suvikunnas, P., J. Salo, and P. Vainikainen, "Impact of power normalization in experimental MIMO antenna performance studies," *IEEE Antennas Wireless Propag. Lett.*, Vol. 6, 43–46, 2007.
40. Suvikunnas, P., J. Salo, L. Vuokko, J. Kivinen, K. Sulonen, and P. Vainikainen, "Comparison of MIMO antenna configurations: Methods and experimental results," *IEEE Trans. Veh. Technol.*, Vol. 57, No. 2, 1021–1031, Mar. 2008.
41. Kildal, P.-S. and C. Orlenius, *Multipath Techniques for Handset/Terminal Antennas*, 4th Edition, Chapter 58, McGraw-Hill Professional, 2007.
42. Jamaly, N. and A. Derneryd, "Efficiency characterisation of multiport antennas," *Elect. Lett.*, Vol. 48, No. 4, 196–198, Feb. 16, 2012.
43. Azremi, A., J. Ilvonen, C. Li, J. Holopainen, and P. Vainikainen, "Influence of the user's hand on mutual coupling of dual-antenna structures on mobile terminal," *Proc. 6th European Conf. Antennas Propag.*, 1222–1226, Mar. 2012.
44. Pozar, D. M., *Mirowave Engineering,* 3rd Edition, John Wiley & Sons, Ltd, 2005.
45. Vaughan, R. and J. B. Andersen, *Channels, Propagation and Antennas for Mobile Communications*, The IEE, 2003.
46. Shiu, D., G. Foschini, M. Gans, and J. Kahn, "Fading correlation and its effect on the capacity of multielement antenna systems," *IEEE Trans. Commun.*, Vol. 48, No. 3, 502–513, 2000.
47. Jensen, M. and Y. Rahmat-Samii, "EM interaction of handset antennas and a human in personal communications," *Proc. IEEE*, Vol. 83, No. 1, 7–17, Jan. 1995.
48. Pedersen, G., K. Olesen, and S. Larsen, "Antenna efficiency of handheld phones," *IEE Seminar Electromagnetic Assessment and Antenna Design Relating to Health Implications of Mobile Phones*, 6/1–6/5, 1999.
49. Plicanic, V., B. K. Lau, A. Derneryd, and Z. Ying, "Channel capacity performance of multi-band dual antenna in proximity of a user," *IEEE Int. Workshop Antenna Technol.*, 1–4, Mar. 2009.
50. Ilvonen, J., R. Valkonen, O. Kivekäs, P. Li, and P. Vainikainen, "Antenna shielding method reducing interaction between user and mobile terminal antenna," *Elect. Lett.*, Vol. 47, No. 16, 896–897, 2011.